

Identification of Néel vector orientation in antiferromagnetic domains switched by currents in NiO/Pt thin films

C. Schmitt^{*1}, L. Baldrati^{*1}, L. Sanchez-Tejerina², F. Schreiber¹, A. Ross^{1,3}, M. Filianina^{1,3}, S. Ding^{1,3,4}, F. Fuhrmann¹, R. Ramos⁵, F. Maccherozzi⁶, D. Backes⁶, E. Saitoh^{5,7,8,9,10}, G. Finocchio², M. Kläui^{1,3}

¹*Institute of Physics, Johannes Gutenberg-University Mainz, 55128 Mainz, Germany*

²*Department of Mathematical and Computer Sciences, Physical Sciences and Earth Sciences, University of Messina, 98166 Messina, Italy*

³*Graduate School of Excellence Materials Science in Mainz, 55128 Mainz, Germany*

⁴*State Key Laboratory for Mesoscopic Physics, School of Physics, Peking University, Beijing 100871, China*

⁵*WPI-Advanced Institute for Materials Research, Tohoku University, Sendai 980-8577, Japan*

⁶*Diamond Light Source, Chilton, Didcot, Oxfordshire OX11 0DE, United Kingdom*

⁷*Institute for Materials Research, Tohoku University, Sendai 980-8577, Japan*

⁸*Advanced Science Research Center, Japan Atomic Energy Agency, Tokai 319-1195, Japan*

⁹*Center for Spintronics Research Network, Tohoku University, Sendai 980-8577, Japan*

¹⁰*Department of Applied Physics, The University of Tokyo, Tokyo 113-8656, Japan*

*These two authors contributed equally to this manuscript.

ABSTRACT

Understanding the electrical manipulation of antiferromagnetic order is a crucial aspect to enable the design of antiferromagnetic devices working at THz frequency. Focusing on collinear insulating antiferromagnetic NiO/Pt thin films as a materials platform, we identify the crystallographic orientation of the domains that can be switched by currents and quantify the Néel vector direction changes. We demonstrate electrical switching between different T-domains by current pulses, finding that the Néel vector orientation in these domains is along $[\pm 1 \pm 1 3.8]$, different compared to the bulk $\langle 11\bar{2} \rangle$ directions. The final state of the Néel vector \mathbf{n} switching after current pulses \mathbf{j} along the $[1 \pm 1 0]$ directions is $\mathbf{n} \parallel \mathbf{j}$. By comparing the observed Néel vector orientation and the strain in the thin films, assuming that this variation arises solely from magnetoelastic effects, we quantify the order of magnitude of the magnetoelastic coupling coefficient as $b_0 + 2b_1 = 3 \times 10^7 \text{ J/m}^3$. This information is key for the understanding of current-induced switching in antiferromagnets and for the design and use of such devices as active elements in spintronic devices.

MANUSCRIPT

Antiferromagnetic materials (AFMs) are promising for spintronic applications, offering several advantages compared to ferromagnets, such as potentially higher switching speeds due to THz resonance frequencies, a higher bit packing density due to the absence of stray fields and increased stability due to the insensitivity to external magnetic fields [1]. The use of AFMs in applications, however, requires an efficient reading and writing of information in defined states of the Néel vector \mathbf{n} . Recently, electrical switching has been reported for both metallic AFMs [2–4] and insulating AFM/heavy metal bilayers [5–11], however, the underlying mechanism, in particular in the latter case, is under debate [5–8]. The different proposals for the switching mechanism depend on the type of domains. So far it is largely unknown which type of domains are present in AFM thin films, for which direction of the Néel vector and,

between which domains the electrical switching occurs. Moreover, the switching can be influenced by mechanisms indirectly related to the injected current flow. For example, the proposed thermomagnetoelastic mechanism for switching relies on a torque via inhomogeneous current-induced temperature gradients generating strain in the thin film via magnetoelastic coupling [8,12]. Among the antiferromagnetic materials where switching has been shown, the most studied to date is NiO, as it provides an ideal platform for spintronic devices. However, the dependence of the magnetoelastic coupling constant on strain in NiO thin films is known only from simulations [13,14], so an experimental estimation is necessary for theoretical models to simulate which effect dominates the switching mechanism.

NiO is a collinear antiferromagnet with a bulk Néel temperature of $T_N = 523$ K [15]. In bulk single crystals, below T_N , NiO contracts along the $\langle 111 \rangle$ directions, forming so called T-domains, leading to the spins being confined to four equivalent ferromagnetic $\{111\}$ planes, coupled antiferromagnetically. Within each of these planes, the spins can orient along one of the three $\langle 11\bar{2} \rangle$ directions (S-domains), leading to a total of 12 possible domain orientations [15–17]. In thin films of NiO grown on MgO, it has previously been discussed that strain induces a preferential out-of-plane orientation of \mathbf{n} with respect to the sample plane [18,19]. On the other hand, many reports of the switching of \mathbf{n} between different states [5,7,18] have used spin Hall magnetoresistance (SMR) measurements, which are sensitive to the in-plane components of \mathbf{n} , and thus indicate the presence of an in-plane component of the Néel vector. It was conjectured that the structure of the magnetic domains in NiO thin films grown on MgO resembles the $[\pm 1 \pm 1 2]$ of the bulk NiO, where only the domains with large n_z , so with large components out of the sample plane, are energetically favorable [18,20,21]. However, a precise determination of the Néel vector direction is missing. The experimental determination of the magnetoelastic coupling constant in particular in thin films has not so far been reported, nor is it clear which types of magnetic domains are involved in the switching of NiO thin films. These pieces of information are key to understand the current-induced switching in antiferromagnets.

In this work, we determine the domain type and the Néel vector orientation of different AFM domains after electrical switching in epitaxial NiO thin films by photoemission electron microscopy (PEEM) employing the x-ray magnetic linear dichroism (XMLD) effect [5,7,22,23]. First, we prepare a state with multiple domains by applying an in-situ electric current pulse in the PEEM setup. Second, by analyzing the XMLD signal as a function of angle between \mathbf{n} and the linear polarization vector, we determine the Néel vector orientation [24], showing that we switch between different T-domains. We further deduce that an electrical pulse along opposite arms of a cross favors a final state with \mathbf{n} orientated parallel to the current pulse. Finally, we determine the order of magnitude of the magnetoelastic coupling coefficient from the alignment of the Néel vector and, by including the strain applied to the NiO thin films by the substrate, show that this is one order of magnitude larger than predicted from DFT calculations [13,14], suggesting that magnetoelastic effects play an important role in the current-induced switching of antiferromagnetic NiO.

We prepared epitaxial MgO(001)//NiO/Pt(2 nm) samples by reactive magnetron sputtering. After pre-annealing the MgO(001) substrates at 770 °C for 2 hours, NiO was deposited from a Ni target at 430 °C and 150 W in an atmosphere of Ar (flow 15 sccm) and O₂ (flow 2 sccm). The platinum layer was subsequently deposited in-situ at room temperature without breaking the vacuum. The epitaxial growth of NiO on MgO (lattice mismatch +0.9%) results in a compressive strain in the out-of-plane direction of the NiO layer (see supplementary Ref. [25]). To be able to apply current pulses, we patterned Hall crosses using optical lithography and subsequent Ar ion etching. The magnetic properties were checked by a polarization-dependent absorption spectrum around the Ni L₂ edge (Fig. 1(a)). The spectrum shows XMLD but no

circular magnetic dichroism (XMCD) signal [26–28], indicating purely antiferromagnetic ordering of the spins with no interfacial ferromagnetic moment. Fig. 1(b) depicts the device layout and the pulsing scheme used for a MgO(001)/NiO(10 nm)/Pt(2 nm) sample, with a 10 μm Pt cross orientated along the [100] crystallographic axes. The contact pads are not symmetric with respect to the axes of the cross, possibly generating a temperature gradient inclined with respect to [100]. The virgin state of this sample was almost single domain (see Fig. 1(c)). Therefore, we first applied a 1 ms-long current pulse with $j = 8.0 \times 10^{11} \text{ A m}^{-2}$ along the [100] direction, generating a three-domain state (Fig. 1(d)). We studied the XMLD signal by varying the incident in-plane angle of the x-rays γ as well as the orientation of the linear polarization ω , both of which are defined in Fig. 1(b). This causes a different contrast between the domains (Fig. 2(a)-(c)) depending on the direction of \mathbf{n} , defined by the in-plane angle ϕ and the out-of-plane angle θ , in each domain and the projection of \mathbf{n} on the linear polarization.

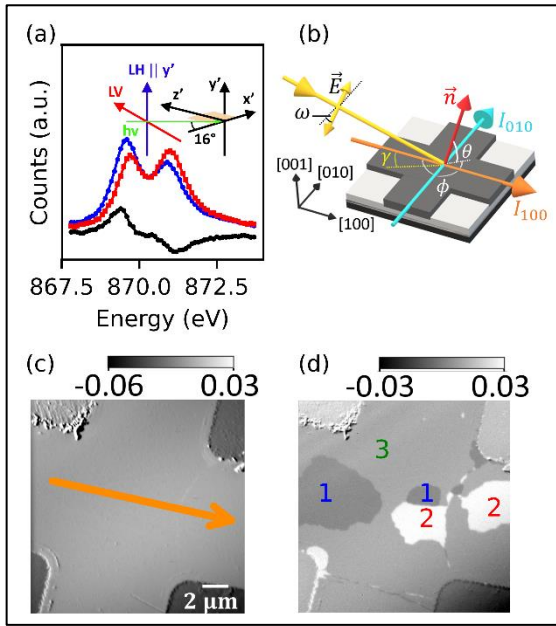


Fig. 1: (a) X-ray absorption spectrum of MgO(001)/NiO(10 nm)/Pt(2) at the Ni L_2 edge for linear vertically (LV) and linear horizontally (LH) polarized light. (b) Device layout and pulsing scheme. The Pt cross is oriented along the [100] crystallographic axes. The angles defining the linear polarization vector and the Néel vector are defined with respect to the crystallographic axes. (c) The virgin state of the sample and (d) the three-level contrast after applying $j = 8.0 \times 10^{11} \text{ A m}^{-2}$ along the [100] direction for 1 ms.

The angular dependent XMLD signal allows us to determine the Néel vector orientation [24]. Fig. 2(d) and (e) show the XMLD signal as a function of the linear polarization ω for $\gamma = 0^\circ$ and $\gamma = -45^\circ$, respectively. The intensity at the absorption edge is given by $I = I_0 + I_1 \cos^2 \alpha + I_2 \cos^2 \beta$, where α is the angle between the linear polarization and \mathbf{n} and β is the angle between the linear polarization and a crystal field component. We assume that the crystal field is along the out-of-plane direction [001] and independent on the spin axes in the domains, as induced by the out-of-plane strain introduced during the growth (see Supplementary Ref. [25]). I_0, I_1 and I_2 are fitting constants related to the XMLD signal. The XMLD-PEEM images in Fig. 2(a)-(c) reveal that, at $\gamma = -45^\circ$, the contrast between domain 1 (blue) and domain 3 (green) reverses twice upon changing the x-ray linear polarization angle. This is also reflected in Fig. 2(e), where the blue and green curves corresponding to the mentioned domains show two points of intersection at $\omega = 12^\circ$ and $\omega = 75^\circ$. These points of

contrast inversion qualitatively and quantitatively determine the relative orientation of the Néel vector in the domains. We fitted the different signals and, considering domains compatible with the NiO domain structure, tetragonal distortion, and contrast inversion points, we determined that there are three different domains with \mathbf{n} along the $[\pm 1.0 \pm 1.0 \ 3.8] \pm [0.1 \ 0.1 \ 0.4]$ directions (Fig. 2(f)) revealing a fourfold in-plane symmetry [18,29]. Based on the symmetry we identify these domains as T-domains, supported by the fact that we also observe them at the oxygen-K edge (See Supplementary Ref. [25]), i.e. they are associated with a domain-dependent crystal field generated by strain. As already reported, for each T-domain, the S-domain with the largest out-of-plane component is favored [18,21], but, compared to the bulk, the out-of-plane Néel vector component is larger, likely due to the lattice expansion in the in-plane crystal direction. Based on the geometry, one expects the fourth T-domain (in-plane angle $\phi = 135^\circ$) to be present as well, but we did not observe it in the investigated sample area. Note that, with a Kerr microscopy based technique at normal incidence, one can see only two contrast levels out of these four domains [12,21,29].

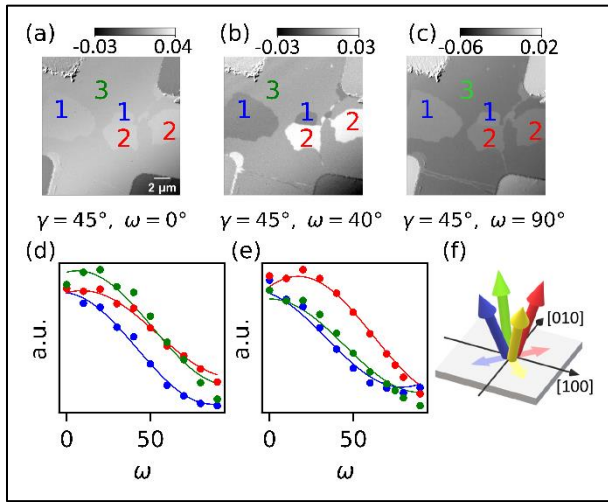


Fig. 2: (a) The three-level contrast for an incident angle of the beam of $\gamma = -45^\circ$ and a polarization $\omega = 0^\circ$. Changing the polarization to (b) $\omega = 40^\circ$ and (c) $\omega = 90^\circ$ changes the relative contrast between the domains. The corresponding XMLD-signal for (d) $\gamma = 27^\circ$ and (e) $\gamma = -45^\circ$ can be fitted including a component stemming from the magnetic signal and an out-of-plane crystal field. (f) The observed domains are T-domains along the four $[\pm 1 \pm 1 \ 3.8]$ directions.

To investigate electrical switching in these samples, we alternated 1 ms-long current pulses between the [100] and [010] directions. The switching threshold along [100] is observed for a current density of $j = 7.5 \times 10^{11} \text{ A m}^{-2}$. A following orthogonal pulse (along [010]), with a slightly lower current density of $j = 7.0 \times 10^{11} \text{ A m}^{-2}$, shows that small regions are switched in all three domains. The difference in the current densities necessary to achieve switching are caused by varying resistances along the two arms leading to different heating. Another pulse along [100] fully reverses the switching (Fig. 3(a)-(c)). Upon increasing the current density, the size of the switched regions increases, reaching saturation at $j = 8.8 \times 10^{11} \text{ A m}^{-2}$ (Fig. 3(d)) along [100]. A perpendicular current pulse creates a quasi mono-domain state (Fig. 3(e)), similar to the virgin state of the sample, favoring the domain with \mathbf{n} orientated along $[\bar{1} \ 1 \ 3.8]$. Another pulse along the [100] direction restores the three-domain state (Fig. 3(f)), showing reproducible current-induced electrical switching for large parts of the sample.

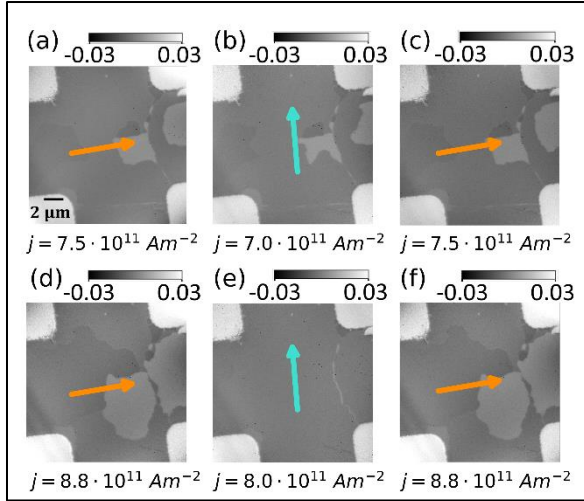


Fig. 3: The application of current pulses at the current threshold alternating between [100] and [010]. (a)-(c) reveals reversible switching of small regions of all three domains. (d) Increasing the current density leads to increased switched regions after a [100] pulse. (e) A perpendicular pulse creates a mono-domain state showing saturation, switching back to the three-level state after a pulse along [100] (f). In all images a background intensity was subtracted.

Next, we check if these Néel vector directions are present in other samples. We patterned a MgO(001)/NiO(5 nm)/Pt(2 nm) sample with a 5 μm Hall cross rotated by 45° and symmetric contact pads with respect to the crystallographic axes, see Fig. 4(a). The cross is aligned along [110], such that current pulses can be applied parallel or perpendicular to the in-plane spin direction. This allows us to determine whether a final state of \mathbf{n} parallel or perpendicular to the applied pulses is favored. Compared to the previous sample, this thinner sample shows smaller but still switchable domains, which we attribute to higher pinning (Fig. 4(c)). We again see a three-level contrast, which we assign to three T-domains with spin directions $[\pm 1 \pm 1 3.8]$ using an analogous procedure as before. The in-plane projection of \mathbf{n} for the three domains, as well as the two possible current pulse directions are shown in Fig. 4(b). Note that domain no. 3 (green), where $\phi = -45^\circ$, is very small. We now observe the T-domain with the Néel vector orientation that was not present in the previous sample (yellow). Applying alternating current pulses along [110] and $[\bar{1}10]$ shows reversible switching (Fig. 4(c)-(e)), but due to higher pinning the switched regions are of smaller size compared to the previous NiO(10 nm)/Pt sample (Fig. 3). Comparing the domain structure before and after applying the electrical pulses, and knowing the Néel vector orientation in each domain shows that the current induced switching favors a parallel alignment of the in-plane Néel vector component \mathbf{n}_{ip} and current pulse direction ($\mathbf{n}_{ip} \parallel \mathbf{j}$), as some of the authors previously reported by electrical SMR measurements [7], which are, however, prone to spurious signals [30].

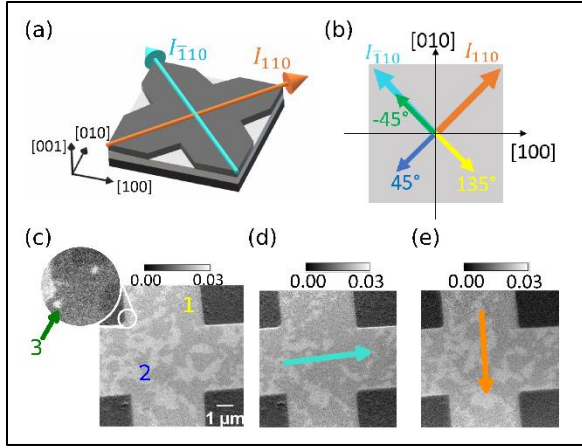


Fig. 4: (a) Device layout and pulsing scheme of the 5 nm NiO film with the Pt cross oriented 45° to the crystallographic axes. (b) Observed in-plane component of Néel vector in the three domains of the NiO(5 nm)/Pt sample and current pulse direction. (c) Domain structure of the virgin state for linear horizontally polarized light. The inset shows a small area of the sample at a different polarization angle ($\omega = 45^\circ$), revealing a third small domain (green). (d) and (e) show the domain structure after 1 ms writing pulses of $j = 1.0 \times 10^{12} \text{ A m}^{-2}$ in two different directions as indicated by the arrows.

In order to extract the quantity that can be used in simulations to understand the switching mechanism, we next estimate the order of magnitude of the magnetoelastic coupling coefficient in NiO. We do this by combining our findings on the Néel vector orientation in the NiO thin films with the strain, induced by the cube-on-cube epitaxial growth that we checked by reciprocal space mapping (see Supplementary Ref. [25]). It is generally accepted that the exchange interaction in NiO is along $\langle 111 \rangle$ (T-domain) and the dipolar interactions keep the spins in the $\{111\}$ planes (along e.g. the $\langle 11\bar{2} \rangle$ directions) [15]. Since the dipolar interaction is not significantly affected by strain [31] and as we observe a small change of the spin orientation compared to the bulk, namely $\langle 113.8 \rangle$ instead of $\langle 11\bar{2} \rangle$, it is reasonable to assume that the small tetragonal distortion along $[001]$, due to the epitaxial growth, contributes to the magnetic anisotropy via the magnetoelastic coupling and favors \mathbf{n} oriented along the compressed axis [31]. As NiO has a large magnetostriction [32], we thus consider only this effect and neglect other crystalline effects and changes in other interactions, allowing us to estimate the order of magnitude of the magnetoelastic coupling. We can express the magnetoelastic energy as $\varepsilon_{me} = K_{ij}^{ME} m_i^\alpha m_j^\alpha$, where K_{ij}^{ME} is the magnetoelastic constant coupling two spins. According to Ref. [13] K_{ij}^{ME} can be expressed as a function of the strain tensor in NiO. The approximation that the off-diagonal elements are zero leads to:

$$\begin{aligned} K_{11}^{ME} &= (b_0 + 2b_1)e_{11} \\ K_{22}^{ME} &= (b_0 + 2b_1)e_{22} \\ K_{33}^{ME} &= (b_0 + 2b_1)e_{33} \end{aligned} \quad (1)$$

Where b_0 and b_1 are the components of the magnetoelastic tensor for NiO, e_{11} , e_{22} are the in-plane strain components and e_{33} is the out-of-plane strain. As shown in the supplementary [25], we measured $e_{11} = e_{22} = 8.6 \cdot 10^{-3} \pm 1.2 \cdot 10^{-3}$, and $e_{33} = -7.1 \cdot 10^{-4} \pm 9.5 \cdot 10^{-4}$ by x-ray diffraction. Combining this with the observed Néel vector orientation of $[\pm 1 \pm 1 3.8]$ and setting the bulk magnetocrystalline anisotropy $K_\alpha^{ME} = 0.25 \text{ MJ m}^{-3}$ [30,33], we used micromagnetic simulations to estimate the sum of the magnetoelastic coefficients required to have the experimentally observed equilibrium position of \mathbf{n} to be $b_0 + 2b_1 = 3 \times 10^7 \text{ J m}^{-3}$ (See supplementary Ref. [25]). This value is an order of

magnitude larger than reported in works based on DFT calculations [13,14]. The sign of the coefficients must also be negative so a compressive (negative) strain enhances the out-of-plane component of the Néel vector. This indicates that the effects due to magnetoelastic coupling can be larger than what was deduced before by DFT calculations, indicating that thermomagnetoelastic switching can be stronger than spin-orbit torques. This estimation, based on experimental results, can be used for future models and to understand quantitatively the role thermomagnetoelastic effects play in the switching mechanism of antiferromagnets.

To conclude, we have observed that the electrical switching of NiO/Pt thin films occurs between different T-domains, demonstrating that the switching process involves magnetoelastic effects and that T-domains can be switched relatively easy, as shown for the bulk [17]. We determined the Néel vector is oriented along the $[\pm 1 \pm 1 3.8]$ directions, canted towards the out-of-plane direction compared to the bulk $[11\bar{2}]$. This effect results from the substrate-induced strain with a magnetoelastic coupling coefficient of value $3 \times 10^7 \text{ J m}^{-3}$. Finally, we determined the final state of the in-plane component of the Néel vector to be parallel to the applied electrical pulse ($\mathbf{n}_{ip} \parallel \mathbf{j}$) in the presence of pulses along $[110]$. By knowing the antiferromagnetic domain structure, magnetoelastic coupling coefficient and the final state after switching, one can compare different switching mechanisms, especially those based on thermomagnetoelastic effects and spin-orbit torques.

ACKNOWLEDGMENTS

L.B acknowledges the European Union’s Horizon 2020 research and innovation program under the Marie Skłodowska-Curie grant agreements ARTES number 793159. L.B., A.R., S.D., M.F. and M.K. acknowledge support from the Graduate School of Excellence Materials Science in Mainz (MAINZ) DFG 266, the DAAD (Spintronics network, Project No. 57334897) and all groups from Mainz acknowledge that this work was funded by the Deutsche Forschungsgemeinschaft (DFG, German Research Foundation) - TRR 173 – 268565370 (projects A01 and B02) and KAUST (OSR-2019-CRG8-4048). M.K. acknowledges financial support from the Horizon 2020 Framework Programme of the European Commission under FET-Open grant agreement no. 863155 (sNebula). We acknowledge Diamond Light Source for time on beamline I06 under proposals MM22448 and MM23819-1. This work was also supported by ERATO “Spin Quantum Rectification Project” (Grant No. JPMJER1402) and the Grant-in-Aid for Scientific Research on Innovative Area, “Nano Spin Conversion Science” (Grant No. JP26103005), Grant-in-Aid for Scientific Research (S) (Grant No. JP19H05600) from JSPS KAKENHI, R.R. also acknowledges support by Grant-in-Aid for Scientific Research (C) (Grant No. JP20K05297) from JSPS KAKENHI, Japan. This work was supported by the Max Planck Graduate Centre with the Johannes Gutenberg Universität Mainz (MPGC).

REFERENCES

- [1] V. Baltz, A. Manchon, M. Tsoi, T. Moriyama, T. Ono, and Y. Tserkovnyak, Antiferromagnetic spintronics, *Rev. Mod. Phys.* **90**, 015005 (2018).
- [2] P. Wadley, B. Howells, J. elezny, C. Andrews, V. Hills, R. P. Campion, V. Novak, K. Olejnik, F. Maccherozzi, S. S. Dhesi, S. Y. Martin, T. Wagner, J. Wunderlich, F. Freimuth, Y. Mokrousov, J. Kune, J. S. Chauhan, M. J. Grzybowski, A. W. Rushforth, K. W. Edmonds, B. L. Gallagher, and T. Jungwirth, Electrical switching of an antiferromagnet, *Science* **351**, 587 (2016).

- [3] S. Yu. Bodnar, L. Šmejkal, I. Turek, T. Jungwirth, O. Gomonay, J. Sinova, A. A. Sapozhnik, H.-J. Elmers, M. Kläui, and M. Jourdan, Writing and reading antiferromagnetic Mn₂Au by Néel spin-orbit torques and large anisotropic magnetoresistance, *Nat. Commun.* **9**, 348 (2018).
- [4] J. Shi, V. Lopez-Dominguez, F. Garesci, C. Wang, H. Almasi, M. Grayson, G. Finocchio, and P. K. Amiri, Electrical manipulation of the magnetic order in antiferromagnetic PtMn pillars, *Nat. Electron.* **3**, 92-98 (2020).
- [5] T. Moriyama, K. Oda, T. Ohkochi, M. Kimata, and T. Ono, Spin torque control of antiferromagnetic moments in NiO, *Sci. Rep.* **8**, 14167 (2018).
- [6] X. Z. Chen, R. Zarzuela, J. Zhang, C. Song, X. F. Zhou, G. Y. Shi, F. Li, H. A. Zhou, W. J. Jiang, F. Pan, and Y. Tserkovnyak, Antidamping-Torque-Induced Switching in Biaxial Antiferromagnetic Insulators, *Phys. Rev. Lett.* **120**, 207204 (2018).
- [7] L. Baldrati, O. Gomonay, A. Ross, M. Filianina, R. Lebrun, R. Ramos, C. Leveille, F. Fuhrmann, T. R. Forrest, F. Maccherozzi, S. Valencia, F. Kronast, E. Saitoh, J. Sinova, and M. Kläui, Mechanism of Néel Order Switching in Antiferromagnetic Thin Films Revealed by Magnetotransport and Direct Imaging, *Phys. Rev. Lett.* **123**, 177201 (2019).
- [8] P. Zhang, J. Finley, T. Safi, and L. Liu, Quantitative Study on Current-Induced Effect in an Antiferromagnet Insulator/Pt Bilayer Film, *Phys. Rev. Lett.* **123**, 247206 (2019).
- [9] I. Gray, T. Moriyama, N. Sivadas, G. M. Stiehl, J. T. Heron, R. Need, B. J. Kirby, D. H. Low, K. C. Nowack, D. G. Schlom, D. C. Ralph, T. Ono, and G. D. Fuchs, Spin Seebeck Imaging of Spin-Torque Switching in Antiferromagnetic Pt/NiO Heterostructures, *Phys. Rev. X* **9**, 041016 (2019).
- [10] Y. Cheng, S. Yu, M. Zhu, J. Hwang, and F. Yang, Electrical Switching of Tristate Antiferromagnetic Néel Order in α -Fe₂O₃ Epitaxial Films, *Phys. Rev. Lett.* **124**, 027202 (2020).
- [11] L. Baldrati, C. Schmitt, O. Gomonay, R. Lebrun, R. Ramos, E. Saitoh, J. Sinova, and M. Kläui, Efficient spin torques in antiferromagnetic CoO/Pt quantified by comparing field- and current-induced switching, *ArXiv:2003.05923 Cond-Mat* (2020).
- [12] H. Meer, F. Schreiber, C. Schmitt, R. Ramos, E. Saitoh, O. Gomonay, J. Sinova, and M. Kläui, Direct imaging of current-induced antiferromagnetic switching revealing a pure thermomagnetoelastic switching mechanism, *arXiv:2008.05219* (2020).
- [13] P. A. Popov, A. R. Safin, A. Kirilyuk, S. A. Nikitov, I. Lisenkov, V. Tyberkevich, and A. Slavin, Voltage-Controlled Anisotropy and Current-Induced Magnetization Dynamics in Antiferromagnetic-Piezoelectric Layered Heterostructures, *Phys. Rev. Appl.* **13**, 044080 (2020).
- [14] T. Nussle, P. Thibaudeau, and S. Nicolis, Coupling magneto-elastic Lagrangians to spin transfer torque sources, *J. Magn. Magn. Mater.* **469**, 633 (2019).
- [15] W. L. Roth, Neutron and Optical Studies of Domains in NiO, *J. Appl. Phys.* **31**, 2000 (1960).
- [16] G. A. Slack, Crystallography and Domain Walls in Antiferromagnetic NiO Crystals, *J. Appl. Phys.* **31**, 1571 (1960).
- [17] W. L. Roth and G. A. Slack, Antiferromagnetic Structure and Domains in Single Crystal NiO, *J. Appl. Phys.* **31**, S352 (1960).
- [18] D. Alders, L. H. Tjeng, F. C. Voegt, T. Hibma, G. A. Sawatzky, C. T. Chen, J. Vogel, M. Sacchi, and S. Iacobucci, Temperature and thickness dependence of magnetic moments in NiO epitaxial films, *Phys. Rev. B* **57**, 11623 (1998).
- [19] S. Altieri, M. Finazzi, H. H. Hsieh, H.-J. Lin, C. T. Chen, T. Hibma, S. Valeri, and G. A. Sawatzky, Magnetic Dichroism and Spin Structure of Antiferromagnetic NiO(001) Films, *Phys. Rev. Lett.* **91**, 137201 (2003).
- [20] S. R. Krishnakumar, M. Liberati, C. Grazioli, M. Veronese, S. Turchini, P. Luches, S. Valeri, and C. Carbone, Magnetic linear dichroism studies of in situ grown NiO thin films, *J. Magn. Magn. Mater.* **310**, 8 (2007).
- [21] J. Xu, C. Zhou, M. Jia, D. Shi, C. Liu, H. Chen, G. Chen, G. Zhang, Y. Liang, J. Li, W. Zhang, and Y. Wu, Imaging antiferromagnetic domains in nickel oxide thin films by optical birefringence effect, *Phys. Rev. B* **100**, 134413 (2019).
- [22] P. Wadley, S. Reimers, M. J. Grzybowski, C. Andrews, M. Wang, J. S. Chauhan, B. L. Gallagher, R. P. Campion, K. W. Edmonds, S. S. Dhesi, F. Maccherozzi, V. Novak, J. Wunderlich, and T.

- Jungwirth, Current polarity-dependent manipulation of antiferromagnetic domains, *Nat. Nanotechnol.* **13**, 362 (2018).
- [23] S.-W. Cheong, M. Fiebig, W. Wu, L. Chapon, and V. Kiryukhin, Seeing is believing: visualization of antiferromagnetic domains, *Npj Quantum Mater.* **5**, 3 (2020).
- [24] S. M. Czekaj, *Ferromagnetic and Antiferromagnetic Domain Configurations in Thin Films and Multilayers: Towards a Patterned Exchange Bias System*, ETH Zurich, 2007.
- [25] Supplementary, (n.d.).
- [26] L. Baldrati, A. Ross, T. Niizeki, C. Schneider, R. Ramos, J. Cramer, O. Gomonay, M. Filianina, T. Savchenko, D. Heinze, A. Kleibert, E. Saitoh, J. Sinova, and M. Kläui, Full angular dependence of the spin Hall and ordinary magnetoresistance in epitaxial antiferromagnetic NiO(001)/Pt thin films, *Phys. Rev. B* **98**, 024422 (2018).
- [27] K. Arai, T. Okuda, A. Tanaka, M. Kotsugi, K. Fukumoto, T. Ohkochi, T. Nakamura, T. Matsushita, T. Muro, M. Oura, Y. Senba, H. Ohashi, A. Kakizaki, C. Mitsumata, and T. Kinoshita, Three-dimensional spin orientation in antiferromagnetic domain walls of NiO studied by x-ray magnetic linear dichroism photoemission electron microscopy, *Phys. Rev. B* **85**, 104418 (2012).
- [28] G. van der Laan, N. D. Telling, A. Potenza, S. S. Dhesi, and E. Arenholz, Anisotropic x-ray magnetic linear dichroism and spectromicroscopy of interfacial Co/NiO(001), *Phys. Rev. B* **83**, 064409 (2011).
- [29] F. Schreiber, L. Baldrati, C. Schmitt, R. Ramos, E. Saitoh, R. Lebrun, and M. Kläui, Concurrent magneto-optical imaging and magneto-transport readout of electrical switching of insulating antiferromagnetic thin films, arXiv:2003.05923 (2020).
- [30] A. Churikova, D. Bono, B. Neltner, A. Wittmann, L. Scipioni, A. Shepard, T. Newhouse-Illige, J. Greer, and G. S. D. Beach, Non-magnetic origin of spin Hall magnetoresistance-like signals in Pt films and epitaxial NiO/Pt bilayers, *Appl. Phys. Lett.* **116**, 022410 (2020).
- [31] M. Finazzi and S. Altieri, Magnetic dipolar anisotropy in strained antiferromagnetic films, *Phys. Rev. B* **68**, 054420 (2003).
- [32] N. B. Weber, H. Ohldag, H. Gomonaj, and F. U. Hillebrecht, Magnetostrictive Domain Walls in Antiferromagnetic NiO, *Phys. Rev. Lett.* **91**, 237205 (2003).
- [33] H. Kondoh and T. Takeda, Observation of Antiferromagnetic Domains in Nickel Oxide, *J. Phys. Soc. Jpn.* **19**, 2041 (1964).
- [34] M. Hutchings and E. Samuelsen, Measurement of Spin-Wave Dispersion in NiO by Inelastic Neutron Scattering and Its Relation to Magnetic Properties, *Phys Rev B* **6**, (1972).